Chapter

An Insight into Biofunctional Curcumin/Gelatin Nanofibers

Nand Jee Kanu, Eva Gupta, Venkateshwara Sutar, Gyanendra Kumar Singh and Umesh Kumar Vates

Abstract

Electrospinning (ESPNG) was used to synthesize ultrathin (UT) and uniform nanofibers (from 5 nm to a few hundred nanometers) of various materials which have biomedical applications (BAs) such as dressing of wounds, drug discharge, and so on and so forth. In the first half of the report, there is an audit on the nanofibers having low diameter so that it could have larger surface area to volume proportion, likewise with that it would have sufficient porosity and improved mechanical properties required for wound healing. Nanofibrous mats (NMs) with high biocompatibility could be utilized during healing of wounds by sustained release of curcumin (Cc) and oxygen. The ESPNG was understood through in-depth numerical investigation in the present report. Furthermore, the process parameters (PMs) were reviewed in depth for their contributions in synthesizing UT - Curcumin/Gelatin (Cc/G) nanofibers (NFs) of optimum diameter. The aim of the discussion was to demonstrate that simply optimizing biofunctional (BF) - Cc/G NFs might not be enough to satisfy experts until they are also given access details about the complete ESPNG method (mathematical mechanism) to improve hold over the synthesis of NMs (suitable for BAs) for the release profile of Cc throughout critical periods of healing process.

Keywords: curcumin/gelatin (Cc/G), nanofibers (NFs), nanofibrous mats (NMs), electrospun (ES), electrospinning (ESPNG), biomedical applications (BAs), methanoic acid (HCOOH)

1. Introduction

1.1 Biofunctional (BF) - curcumin/gelatin (cc/G) nanofibers (NFs)

The impact of new revelations in the field of nanotechnology widespreadly affects the wellbeing sciences (**Table 1**). In biomedical field, the possible parts of NFs applications which resemble drug delivery and tissue science and medicine have been researched in the article. In spite of the fact that electrospinning (ESPNG) was considered as a reasonable system for the polymer nanofibers that were polymeric, biodegradable or non-biodegradable, manufactured or common and so on, which were with uniform distances across ranges from 5 nm to a few hundred nanometers [2–4]. The ESPNG procedure was favored over other regular strategies in published papers for the synthesis of polymer nanofibers [5–8]. The requirements for the biopolymers such as their restricted dissolvability in natural

Few ES - NFs loaded with Cc	Potential application in wound healing/ dressing, so on
Few Cc loaded NFs including (a) polycaprolactone-polyethylene glycol; (b) poly (3-hydroxybutyric acid-co-3-hydroxyvaleric acid) (PHBV); (c) poly(lactic acid) hyperbranched polyglycerol; (d) $\varepsilon-$ polycaprolactone/ polyvinylalcohol; and so on	Potential wound healing application
Few Cc loaded NFs including tragacanth/ poly(ε-caprolactone) NFs	Potential application in dressing of diabetic wound based on *in vivo*
Few Cc loaded NFs including almond gum/ polyvinyl alcohol (PVA) NFs	Therapeutic capacity and bioavailability
Few Cc loaded NFs including Zinc-Cc with coaxial NFs	Orthopedic applications
Few Cc loaded NFs including (a) zinc NFs; (b) cellulose acetate/ polyvinylpyrrolidone NFs; (c) polyurethanes NFs; (d) gelatin (G) NFs; and so on	Antibacterial application
Few Cc loaded NFs including chitosan/ poly (vinyl alcohol) (PVA) NFs; and so on	Sustained drug release

Table 1.
Potential applications of biofunctional (BF) - curcumin (cc) based electrospun (ES) NFs (reprinted with permission from ref. [1]. Copyright 2020 IOP publishing).

solvents due to high particle size, as well as their expensive purifying steps and their suitable polymeric solutions because of their inclination to frame hydrogen bonds, were controlled subsequent to mixing with engineered polymers in any case these restrictions may limit their ESPNG process for nanofibrous mats (NMs) [9].

The nanofibrous mats (NMs) which were prepared from ES collagen nanofibers were utilized for applications of tissue science and medicine [8]. Additionally, *Aloe vera* which is a characteristic polymer also holds potential to be used for tissue science and medicine applications because it has a cancer prevention agents and it is totally not harmful to living tissues [10, 11]. The BAs of some other ES nanofibers were discussed in **Table 1**. Gelatin (G), a polymer made up of proteins and peptides, is not harmful to living tissues. As a result, it was thought to be a fair and healthy option when it came to dressing dangerous injuries, such as diabetic ulcers.

Due to their considerable tensile strength compared to traditional fibers (with diameters ranging over 100 nm), the low profile NFs can serve as a suitable material while healing and act as barriers to protect the wound (**Figures 1** and **2**) [11–14]. Gelatin is also noted for its high water absorption and fluid affinity, making it an ideal option for the moist healing process. In methanoic acid, gelatin (a natural biopolymer that is a denatured form of collagen) is quite soluble. Collagen is a protein found in the extracellular matrix (ECM) of humans and animals, but it is costly due to its production processes [15–25]. The properties of these nanofibers can also be regulated according to requirements by optimizing input process parameters (PMs) such as high potential power supply, solution's resistance to the flow, length between the NFs collector and emitter, and feed rate, according to the authors. Methanoic acid was clearly used as a natural unstable dissolvable in the ESPNG to disintegrate gelatin (G) at room temperature. Recently, the use of G-nanofibers with sufficient tensile strength for fabricating NMs has got a lot of attention for antimicrobial applications [26–30]. In addition to their light weight (LW), effective spinning of minimum diameter nanofibers provides a large surface area of these nanofibers. It was fundamentally required for the purpose of dressing the wounds and for other BAs (**Table 1**). Mindru et al. [31] succeeded in synthesizing NMs of sufficient strength for BAs using methanoic acid. Rather than cytotoxic

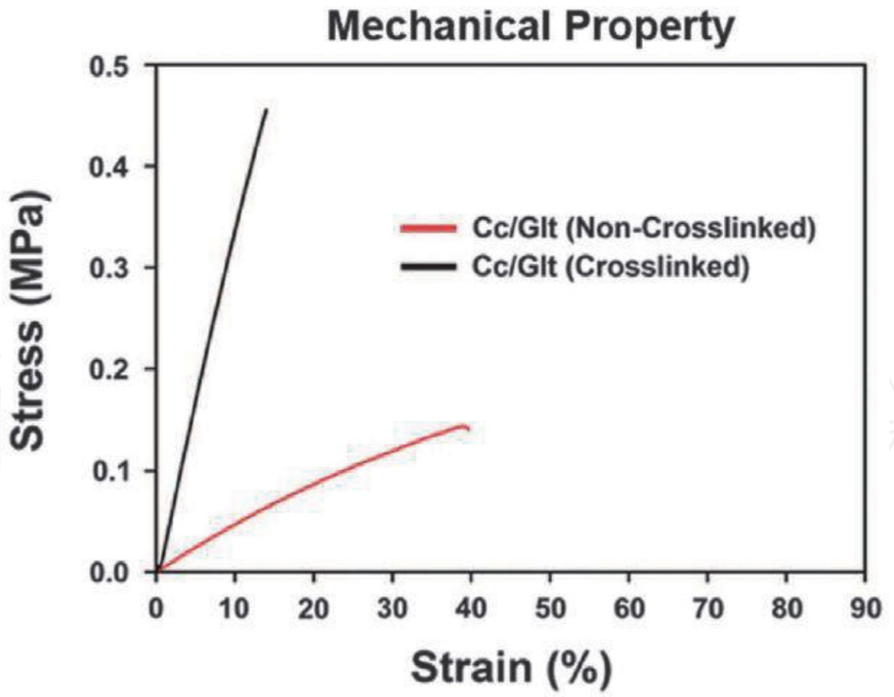

Figure 1.
The BF - ES NFs were crosslinked to improve tensile strength of the NMs (reprinted with permission from ref. 12. Copyright 2017 springer nature).

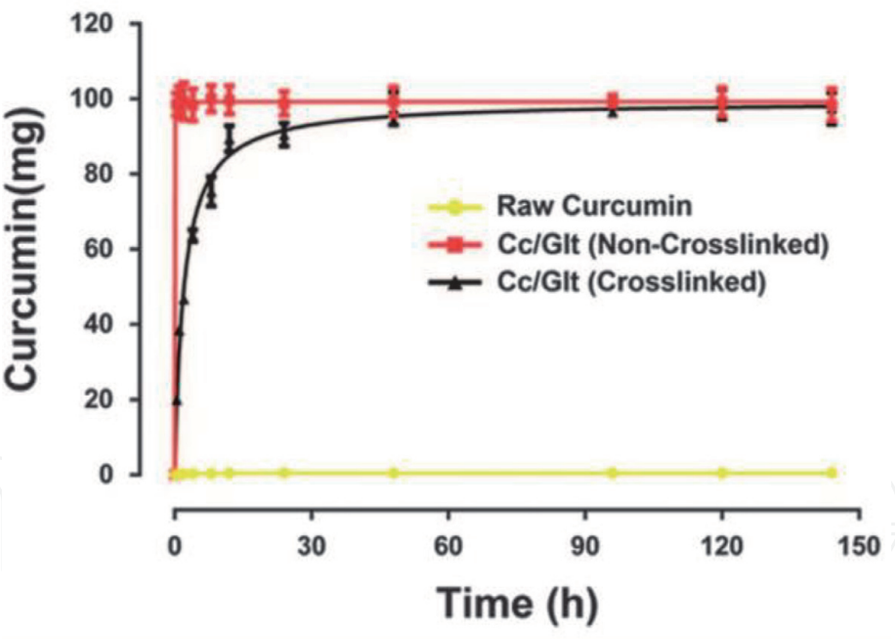

Figure 2.
The event of cc discharge was shown with time (reprinted with permission from ref. 12. Copyright 2017 springer nature). The need to crosslink the ES - NFs was illustrated.

solvents, Maleknia et al. [32] utilized HCOOH/water to get ready solutions for the ESPNG of G-nanofibers which can be utilized for BAs such as dressing of wounds, delivery of pharmaceuticals, and for tissue science and medicine. They were successful in synthesizing G-nanofibers with 197 nm diameter. Chen et al. [33] utilized methanoic acid and ethanol to have the improvement in the volatility of the dissolvable rather than cytotoxic solvents while setting up the dissolvable for preparing ES G-nanofibers. For medication conveyance, the nanofibrous mats broke in a rapid manner in fluid polymeric solutions. Aytac et al. [23] research suggests that ES

G-NFs exemplified with ciprofloxacin/hydroxypropyl-beta-cyclodextrin incorporating complex will break down quicker in water than ES G-nanofibers stacked with ciprofloxacin. Using a dialysis process, Yabing et al. [21] synthesized drug-loaded micelles (poly(ethylene glycol)-block-caprolactone copolymer) and integrated these pharmaceuticals into ES G-NFs. The NMs developed using ES NFs have considerable surface regions and such NFs have a significant contribution in tissue science and medicine. The solvent utilized here was the methanoic acid for ESPNG BF-nanofibers which leads to different BAs such as enzyme immobilization, materials for bone recovery, antifungal and antibacterial exercise in the release of medications, bioactive materials encapsulation during packaging of food and dressing of wounds [34].

The turmeric extracted from *Curcuma longa*, which was regular turmeric (herbaceous plant) and is broadly utilized in Asian countries like India and China, as a bioactive compound with potent anti-inflammatory and antioxidant properties in medicine. Synthetic dimethoxycurcumin has been found to be more effective than natural curcumin (Cc) at destroying cancer cells (which is the leading cause of death in the world) (derived from the plant) [35–45]. Ramrezagudelo et al. [36] incorporated antibiotic doxycycline pharmaceuticals (mitochondrial biogenesis inhibitors that may limit cancer stem cells in the early stages of breast cancer) into ES hybrid poly-caprolactone/gelatin/hydroxyapatite soft NMs and assessed these drug delivery meshes as effective antitumor and antibacterial scaffolds (**Figure 3**). The utilization of methanoic acid as dissolvable for solutes such as Cc and gelatin (G) has been the favored decision in numerous BAs. Researchers have successfully prepared solutions of Cc and dimethoxycurcumin utilizing methanoic acid [35, 46–48]. After 12 hours, higher concentrations of Cc, such as 17 percent Cc loaded poly (ε-caprolactone) (PCL) NFs, should release more Cc at a particular rate than lower concentrations such as 3 percent Cc loaded PCL NFs. (**Figure 2**) [11, 12]. Utilization of PCL-Cc polymeric solutions, BF-ES nanofibers were prepared [11–14, 48].

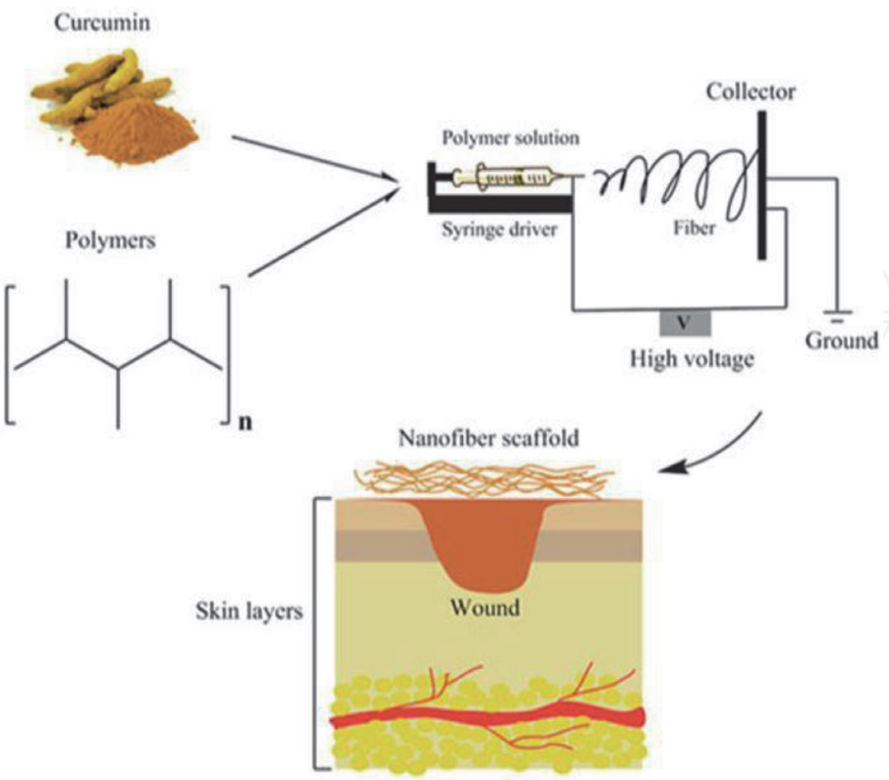

Figure 3.
Preparation of cc loaded ES NFs for sustained release of pharmaceuticals for potential healing process (reprinted with permission from ref. 13. Copyright 2018 John Wiley and Sons).

Xinyi et al. [12] synthesized curcumin/gelatin (Cc/G) nanofibrous mats and studied the arrival of Cc on rodent models (intense injury) by means of an in vitro approach. The healing process was tested by treating rodents utilizing the Cc/G nanofibrous mats (investigations done on the third, seventh, and fifteenth days subsequent to injuring). It inspired us to create Cc-loaded gelatin NFs suitable for the fabrication of NMs for the application of Cc and oxygen to the wound on a long-term basis (during healing) [13]. These NMs will then have antioxidant and anti-inflammatory properties, making them ideal for the healing process [13, 48–66].

1.2 Mechanism behind electrospinning (ESPNG) of cc/G nanofibers (NFs)

The process of electrospinning (ESPNG) utilizes an electric field applied to the emitter and a ground terminal to pull back a thread of polymeric solution out of the opening of the emitter. In the process of ESPNG, the Maxwell electrical pressure was set as per ratio, $\frac{V^2}{d^2}$; where permittivity was $'\varepsilon'$, a high potential power supply was $'V'$ and the electrode spinning gap was shown with $'d'$. The critical high potential power supply (V_c) was $\sqrt{\frac{\gamma d^2}{\varepsilon R}}$, and it must exceeded before any jet could spread out from the needle tip. For, $\gamma = 10^{-2} kg/s^2, d = 10^{-2} m, \varepsilon = 10^{-10} C^2/(Jm)$ $and R = 10^{-4} m$, a high potential power supply around 10 KV was necessary to form a jet of any type. The polymeric solution of the Laplace condition (utilized in the modeling) in the feeble polarization limit depicts the electrostatics in the fluid stage in an axisymmetric indirect support framework (r, θ, ϕ) with the vertices of the Taylor cone at the source which can be shown using general Eq. (1).

$$\begin{aligned} \psi_1(r,\theta) &= A_n r^n P_n(\cos\theta); for \theta_0 \geq \theta \geq 0, \\ \psi_g(r,\theta) &= B_n r^n P_n(\pi - \theta); for \pi \geq \theta \geq \theta_0 \end{aligned} \tag{1}$$

Eq. (1), $V = \frac{4}{3}\pi r^3$, was the drop in the volume of fluid, here the spinning gap r which was from the cone vertex of angle $2\theta_0$ to the emitter tip and the state of the drop was said to be utilizing a Taylor cone, accordingly was described as $r = R(z)$. Later on the z- axis was corresponding to the applied electric field with $z \in [-l, l]$, where l was the length if the semi-long pivot of the drop and limit condition $\theta_0 \geq \theta \geq 0$ represents the boundary condition of the fluid. $P_n\ [x]$ was the Legendre's function, where A_n and B_n were constants. They suggested a model for ESPNG polymeric nanofibers which relies upon a sink-like flow towards the vertex of the Taylor cone. The course of action of the flow in axisymmetric polar headings $(r, \varepsilon, 0)$ was given utilizing conditions (2) and (3).

$$v_r = \frac{vF(\varepsilon)}{r} \tag{2}$$

$$F(\varepsilon) = b\left\{3\tanh^2\left[\left(\sqrt{\frac{-b}{2}}\right)(\alpha - \varepsilon) + 1.146\right] - 2\right\} \tag{3}$$

In the above Eqs. (2) and (3), velocity of the radial feed, v_r, the kinematic solution's resistance to the flow of feed, v, the wedge/Taylor cone half angle, a, the parameter, b which serves to decides the inertial concentration of stream on the Taylor cone vertex/Taylor cone. With that the mass and charge conservations led to expressions for v and σ in terms of R and E, also the force and E-field conditions were assessed utilizing second-degree differential equations. Inclination of the stream surface (R) was supposed as the highest from the origin of the nozzle and

hence the initial result of z was equal to zero. Furthermore, PMs were discussed using the set of Eqs. (4) [67, 68].

$$\begin{aligned} R(0) &= 1 \\ E(0) &= E_0 \\ \tau_{prr} &= 2r_n \frac{R_0'}{{R_0}^3} \\ \tau_{pzz} &= -2T_{prr} \end{aligned} \tag{4}$$

Here Eq. (4), the radius of the jet initially was $'R_0'$ and the formula used for calculating the jet velocity, $\upsilon_0 = \frac{Q}{\pi R_0^2 K}$, where the rate of discharge of the polymeric solution, Q, and the conductivity of the liquid solution, K. Moreover, the electric field (E_0) was calculated using the formula, $E_0 = \frac{I}{\pi R_0^2 K}$ and the surface charge density (σ_0) was calculated using the formula, $\overline{\varepsilon} E_0$, where the dielectric constant of ambient air was $'\overline{\varepsilon}'$ and the constant was $'E_0'$ which was to be used during simulation of the ESPNG. The viscous stress (τ_0) was calculated using the formula, $\tau_0 = \frac{\eta_0 \nu_0}{R_0}$. A Newtonian liquid law of force for the liquid was summed up and for that the shear pressure (τ) was given as $\tau = K\left(\frac{\partial v}{\partial y}\right)^m$ as shown using Eq. (5) [67]. The electric field will overcome the surface tension of the polymer liquid and thereafter through Taylor's cone NFs will be pulled out and ES over the moving cylinder collector.

$$\frac{d(\sigma R)}{dz} \simeq -\left(2R\frac{dR}{dz}\right)/Pe \tag{5}$$

Furthermore, the response of $'E'$ is a function of axial position (z) and it can be shown in Eq. (6) [1, 69, 70].

$$\frac{d(E)}{dz} = \ln\chi\left(\frac{d^2R^2}{dz^2}\right)/Pe \tag{6}$$

The model discussed above so far was found fit for foreseeing the conduct of the PMs of the ESPNG [67].

2. Electrospinning (ESPNG) of cc/G nanofibers (NFs)

In the present investigation, we utilized set-up for ESPNG (**Figure 4(a)**). The prominent four parts that were related to the ESPNG – PMs such as spinning gap between the emitter and drum collector, high potential power supply, rate of feed, and solution's resistance to the flow of a polymeric solution (taken in a 2 ml needle syringe). For the ESPNG process, a high potential power supply has been set across the length of the moving cylindrical drum collector (covered with an aluminum sheet) to pull NFs from Taylor's cone formed at the tip of the syringe's needle. The NFs were stretched up from the polymeric solution containing a polar natural solvent and a polymer solute in a definite proportion. After that, these NFs were collected over the moving cylinder which was turned with a speed of around 1000 rpm so that the NFs with UT - diameters could be synthesized across by

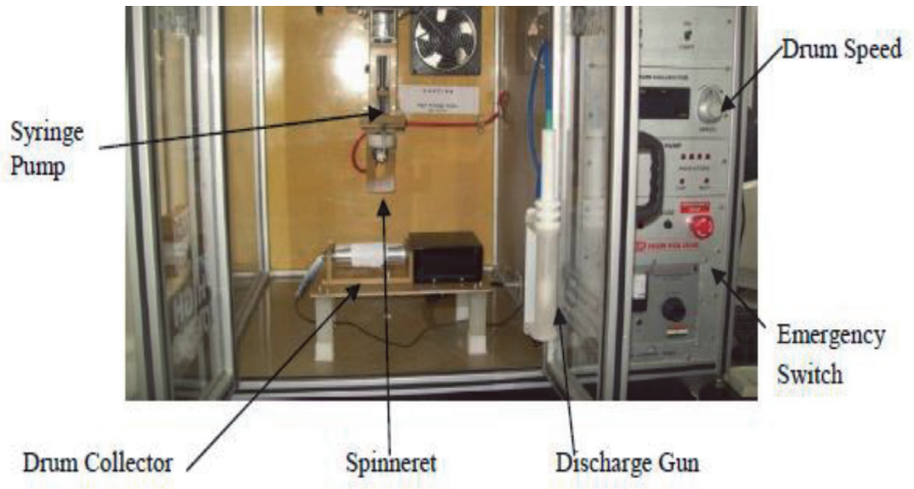

(a)

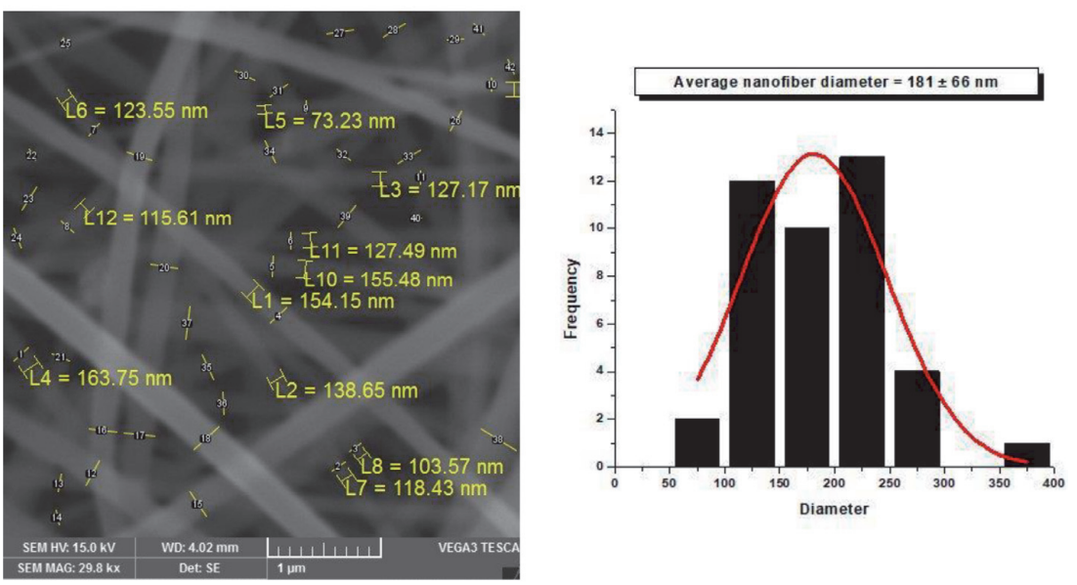

(b)

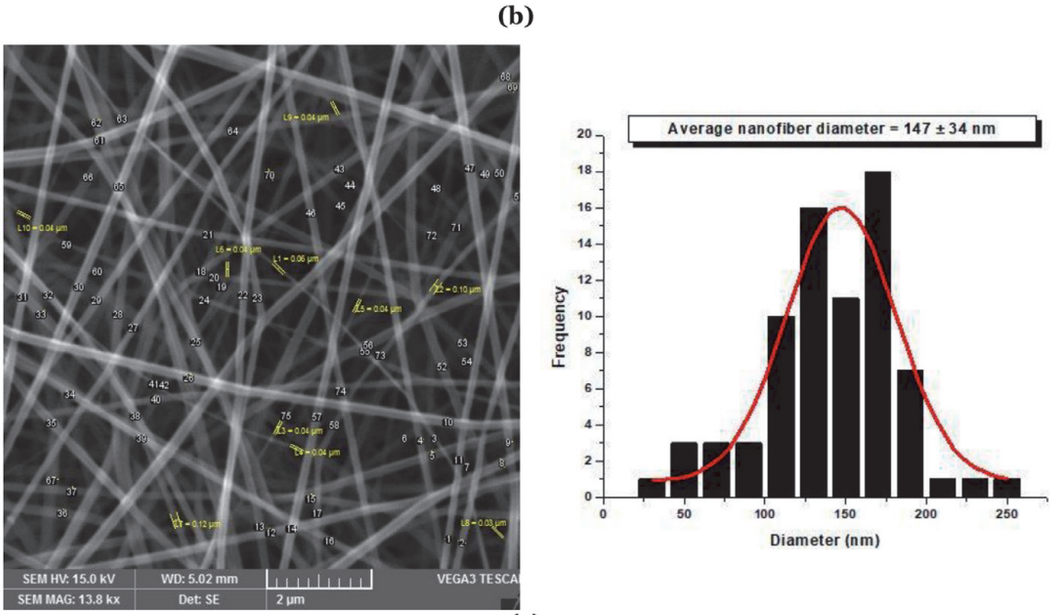

(c)

Figure 4.
The (a) ESPNG set up was used to synthesize (b), and (c) the UT - and BF - Cc/G NFs (Reprinted with permission from Ref. [70]. Copyright 2020 IOP Publishing).

extending them and adjusting them directly as well as improving their mechanical properties. The four PMs were the spinning gap between the collector and needle's tip, rate of feed, solution's resistance to the flow, and the high potential power supply were considered [1, 69, 70].

For synthesizing the BF - NFs parameters were considered. The polymeric solution was prepared after blending 1 percent curcumin (Cc) (0.1 g) with 1.5 percent G (0.15 g) in 10 ml of methanoic acid (98 percent concentrated). Other than that, each other polymeric solution was prepared by mixing 1.2 percent Cc (0.12 g) with 2 percent G (0.2 g) in 10 ml of methanoic acid (98 percent concentrated), both at room temperature. The examinations were done at room temperature, in encompassing air which had moisture around 80 percent.

The synthesis of NFs was done by varying the spinning gap between the tip of the needle (10 cm and 15 cm), the rate of feed (0.1 ml h^{-1} and 0.15 ml h − 1), the possible high potential power supply (15 KV and 20 KV), and the solution's resistance to the flow (65 cP and 70 cP, on account of the additional substances obsessions). For 48 hours, the mats were dried at room temperature to completely remove the methanoic acid. The diameters of the NFs were then examined using scanning electron microscopy (SEM) (**Figure 4(b)**, and **(c)**).

3. The electrospun (ES) cc/G nanofibers (NFs): a state-of-the-art review

The diameter (nm) of the NFs was synthesized during the process of electro spinning measures (**Table 2**). The differences in the outcomes (as far as the

Runs	Spinning gap (cm) A	Feed Rate (ml/h) B	High potential power supply (KV) C	Solution's resistance to the flow (cP) D	Mean Diameter (nm)
1	Low - 10	Low - 0.1	Low - 10	Low - 65	***205 ± 22.5***
2	High - 15	Low - 0.1	Low - 10	Low - 65	***181 ± 66***
3	Low - 10	High - 0.15	Low - 10	Low - 65	***270 ± 16***
4	High - 15	High - 0.15	Low - 10	Low - 65	***280 ± 20***
5	Low - 10	Low - 0.1	High - 15	Low - 65	***260 ± 26.5***
6	High - 15	Low - 0.1	High - 15	Low - 65	***254 ± 28***
7	Low - 10	High - 0.15	High - 15	Low - 65	***147 ± 34***
8	High - 15	High - 0.15	High - 15	Low - 65	***286 ± 31***
9	Low - 10	Low - 0.1	Low - 10	High - 70	***287 ± 77***
10	High - 15	Low - 0.1	Low - 10	High - 70	***288 ± 57***
11	Low - 10	High - 0.15	Low - 10	High - 70	***375 ± 96***
12	High - 15	High - 0.15	Low - 10	High - 70	***206 ± 56***
13	Low - 10	Low - 0.1	High - 15	High - 70	***308 ± 74***
14	High - 15	Low - 0.1	High - 15	High - 70	***229.5 ± 60***
15	Low - 10	High - 0.15	High - 15	High - 15	***235 ± 47***
16	High - 15	High - 0.15	High - 15	High - 70	***274 ± 53***
					Total $\sum X = 4085.5$

Table 2.
The effect of PMs on diameters of cc/G NFs (reprinted with permission from ref. 1. Copyright 2020 IOP publishing).

diameters of the NFs) synthesized were as per the following: at a high potential power supply such as 15 KV (at 15 cm distance, 0.1 ml h^{-1} rate of feed and 65 cP solution's resistance to the flow) utilizing a solution having 1.5 percent G, 1 percent Cc in 10 ml of 98 percent concentrated methanoic acid, NFs with diameters around 254 nm (254 ± 28 nm) which was quite larger than the 181 nm (181 ± 66 nm) (**Figure 4(b)**) spinning gap across got at 10 KV using similar polymeric solution and keeping PMs at same levels. At a higher rate of feed such as 0.15 ml h^{-1} (at 10 cm distance, 15 KV high potential power supply, and 65 cP solution's resistance to the flow) utilizing a solution having 1.5 percent G, 1 percent cc in 10 ml of 98 percent concentrated methanoic acid, the diameter across of NFs were prepared around 147 nm (147 ± 34 nm) (**Figure 4(c)**) which was quite smaller than 260 nm (260 ± 26.5 nm) as the diameter synthesized at 0.1 ml h^{-1} rate of feed utilizing similar polymeric solution and keeping PMs at same levels. At a higher rate of feed such as 0.15 ml h^{-1} (at 15 cm distance, 10 KV power supply, and 70 cP solution's resistance to the flow) utilizing an solution having 2 percent G, 1.2 percent Cc in 10 ml of 98 percent concentrated methanoic acid, the diameter of NFs were prepared around 206 nm (206 ± 56 nm) which was smaller than 229.5 nm (229.5 ± 60 nm) as the diameter synthesized at 0.1 ml h^{-1} (at 15 cm distance, 15 KV high potential power supply and 70 cP solution's resistance to the flow) utilizing a similar polymeric solution. For a higher concentration (2 percent G, 1.2 percent Cc in 10 ml of 98 percent concentrated methanoic acid), the solution's resistance to the flow was prepared (utilizing a solution's resistance to the flow - measurement set up) to be 70 cP and afterward the diameter of the NFs increased to 235 nm (235 ± 47 nm) at 10 cm distance, 0.15 ml h^{-1} rate of feed and 15 KV high potential power supply, from 147 nm (147 ± 34 nm) (**Figure 4(c)**) (prepared at 1.5 percent G, 1 percent Cc in 10 ml of 98 percent concentrated methanoic acid) at 10 cm distance, 0.15 ml h^{-1} rate of feed, 15 KV high potential power supply and 65 cP solution's resistance to the flow. At a spinning gap between the collector and needle's tip such as 15 cm (0.15 ml h^{-1} rate of feed, 15 KV high potential power supply, and 70 cP solution's resistance to the flow) utilizing an solution having 2 percent G, 1.2 percent Cc in 10 ml of 98 percent concentrated methanoic acid, the diameters of NFs were prepared around 274 nm (274 ± 53 nm) which was larger than the 235 nm (235 ± 47 nm) diameter obtained for 10 cm spinning gap utilizing similar polymeric solution and keeping PMs at same levels [1, 69, 70].

3.1 Design of experiments

The 2^k factorial design algorithm was run to test the basic variables or PMs such as the gap between collector and needle's tip, rate of feed, high potential power supply, and solution's resistance to the flow (each changed at two unique levels such as low (−) and high (+)) [71–73]. Accordingly, the total number of runs or trials were 2^4 i.e., 16. Each of the 16 examples was inspected under scanning electron microscopy (SEM) for characterization of diameters in *nm* (as listed in **Table 2**). A few samples of the Cc/G NFs analyzed under SEM were shown in **Figure 4(b)**, and **(c)**). The UT – spongy NMs were synthesized under all process conditions [1, 69, 70].

3.2 Analysis of variance

Analysis was performed to find the effects of PMs on the diameter of BF nanofibers. Correction factor, CF (to calculate the sum of squares of PMs) was evaluated using relationship (7).

3.2.1 Correction factor (CF)

For diameter (nm), the correction factor (CF) was calculated as

$$CF = \frac{(\Sigma X)^2}{n} = \frac{(4085.5)^2}{16} \cong 1043207 \tag{7}$$

Where the gross total of observed diameters ΣX and the number of iterations n, was 16.

The effect of the factors can be assessed using Eq. (8).

$$\frac{[\Sigma Y_{low}]^2}{n} + \frac{[\Sigma Y_{high}]^2}{n} - CF \tag{8}$$

Where Y is an input variable such as the spinning gap (A), Y_{high} and Y_{low} represents the aggregate of all mean diameters synthesized at low (−)and high (+) levels, individually, for the specific info variable with each whole assumed control over the high and low estimations of different factors. The mean diameters for the low (−) and high (+) levels of PMs were taken from **Table 2** [1, 69, 70].

1. Sum of squares, spinning gap variable (cm),SS_A

$$\begin{aligned}
&\frac{[\Sigma A_{low}]^2}{n} + \frac{[\Sigma A_{high}]}{n} - CF \\
&= \frac{[205 + 270 + 260 + 147 + 287 + 375 + 308 + 235]^2}{8} \\
&+ \frac{[181 + 280 + 254 + 286 + 288 + 206 + 229.5 + 274]^2}{8} - 1043207 \\
&= 489.5
\end{aligned}$$

The sum of the square of any interaction was assessed using Eq. (9).

$$\frac{[\Sigma AB_{low}]^2}{n} + \frac{[\Sigma AB_{high}]^2}{n} - CF \tag{9}$$

For any interaction such as AB, the SS_{AB} was evaluated as follows:

2. Sum of squares for interaction AB, SS_{AB}

$$\begin{aligned}
&\frac{[\Sigma AB_{low}]^2}{n} + \frac{[\Sigma = AB_{high}]^2}{n} - CF \\
&= \frac{[181 + 270 + 254 + 147 + 288 + 375 + 229.5 + 235]^2}{8} + \\
&\frac{[205 + 280 + 260 + 286 + 2870206 + 308 + 274]^2}{8} - 1043207 \\
&= 1000
\end{aligned}$$

Out of all interactions, the SS_{ABC} was recorded for its *highest result* around *9925.* The errors were added together and the ratio, MS_{error} was calculated using Eq. (10).

$$MS_{error} = SS_{error}/V_{error} = 21 \tag{10}$$

Where, representation of the number of errors was done by V_{error}, and in our case it was one. Now, ratio which was calculated, using the *F*-distribution Table, which was *F* esteemed for 95 percent degree of certainty as 7.71 and further inferred that the diameter relies on factors: (a) - Interaction between spinning gap (cm), (ml h^{-1}) rate of feed and (KV) high potential power supply, (b) - Interaction between spinning gap (cm) and solution's resistance to the flow (cP), (c) D-Solution's resistance to the flow (cP), (d) - Interaction between rate of feed (ml h^{-1}) and high potential power supply (KV), (e) - Connection between spinning gap (cm) and high potential power supply (KV), (f) - Interaction between rate of feed (ml h^{-1}), high potential power supply (KV) and solution's resistance to the flow (cP), (g) - Interaction between spinning gap (cm), (ml h^{-1}) rate of feed, (KV) high potential power supply and solution's resistance to the flow (cP), (h) - Interaction between spinning gap (cm) and rate of feed (ml h^{-1}), (I) - Interaction between high potential power supply (KV) and solution's resistance to the flow (cP), (j) - Interaction between rate of feed (ml h^{-1}) and solution's resistance to the flow (cP), (k) - High potential power supply (KV), (l) A - spinning gap (cm), and (m) - Rate of feed (ml h^{-1}).

3.3 Regression analysis

Every process parameter here has two levels such as low (−) and high (+) levels and a degree of freedom (DOF), in this way we utilized a common regression model to compute the minimum diameter of NFs based on the effects of interactions such as $\beta_1, \beta_2, \beta_3, \beta_4, \beta_5, \beta_6, \beta_7, \beta_8, \beta_9$ and β_{10} (in terms of contributions of interactions between *ABC*-Interaction between spinning gap (cm), rate of discharge of polymeric solution (ml h^{-1}) and high potential power supply (KV), *AD* -Interaction between spinning gap (cm) and solution's resistance to the flow (cP), *BC* - Interaction between rate of discharge of polymeric solution (ml h^{-1}) and high potential power supply (KV), *AC* -Interaction between spinning gap (cm) and high potential power supply (KV), *BCD* - Interaction between rate of discharge of polymeric solution (ml h^{-1}), high potential power supply (KV) and solution's resistance to the flow (cP), *ABCD* - Interaction between spinning gap (cm), rate of discharge of polymeric solution (ml h^{-1}), high potential power supply (KV) and solution's resistance to the flow (cP), *AB* -Interaction between spinning gap (cm) and rate of discharge of polymeric solution (ml h^{-1}), *CD* - Interaction between high potential power supply (KV) and solution's resistance to the flow (cP), *BD*-Interaction between rate of discharge of polymeric solution (ml h^{-1}) and solution's resistance to the flow (cP), respectively) as well as the main effects such as $\beta_3, \beta_{11}, \beta_{12,}$ and β_{13} (in terms of contributions of *D* - Solution's resistance to the flow (cP), *C* - High potential power supply (KV), *A* -Spinning gap (cm), and *B* - rate of discharge of polymeric solution (ml h^{-1}), respectively), in Eq. (11).

$$Y(T_n) = \beta_0 + \beta_1 T_1 + \beta_2 T_2 + \beta_3 T_3 + \ \ldots \ + \beta_n T_n + \eta \tag{11}$$

Where,

$$\beta_0 = \sum_{i=1}^{N} \frac{Y_i}{N} = \frac{4085.5}{16} = 255.344$$

Furthermore, the influence of each process parameter, *P*, was computed using the relationship, $Y_P = \bar{Y}_{P+} - \bar{Y}_{p-}$, where $\bar{Y}_{P+}$ and $\bar{Y}_{p-}$ stand for the sum of all mean diameters prepared at low (−) and high (+) levels, respectively, for the particular

input variable. The results of the corresponding mean diameters for the low (−) and high (+) levels of the particular process parameter were taken from **Table 2**.

Therefore, the percentage contribution for ABC = $(9925/41257.5) \times 100 = 24$.

$\beta_1 = \frac{1}{2} \times$ The influence of the interaction, ABC= 25.

The general form of the regression equation was formulated and shown in Eq. (12). Using Eq. (12), the minimum diameter of curcumin/gelatin (Cc/G) NFs (nm) for sustained release of Cc could be evaluated after determination of the coefficients (such as $\beta_1, \beta_2, \beta_3, \beta_4, \beta_5, \beta_6, \beta_7, \beta_8, \beta_9$ and β_{10}) of the interaction effect (such as $X_{ABC}, X_{AD}, X_{BC}, X_{AC}, X_{BCD}, X_{ABCD}, X_{AB}, X_{CD}$ and X_{BD}) as well as the coefficients (such as $\beta_3, \beta_{11}, \beta_{12,}$ and β_{13}) of the basic PMs (such as $X_D, X_C, X_{A,}$ and X_B).

$$\begin{aligned}\text{Diameter (nm)} = {} & 255.344 + 25X_{ABC} - 20.5X_{AD} + 20X_D - 17.75X_{BC} + 17.25X_{AC} + 13X_{BCD} \\ & + 11X_{ABCD} + 8X_{AB} - 7.5V_{CD} - 6.5X_{BD} - 6X_C - 5.5X_A + 3.75X_B \end{aligned} \tag{12}$$

The above model Eq. (12) was valid for the boundary conditions such as (a) $10 \le X_A \le 15$ (cm), (b) $0.10 \le X_B \le 0.15$ (ml h^{-1}), (c) $10 \le X_c \le 15$ (KV), (d)$65 \le X_D \le 70$ (cP).

The mean diameters (nm) of Cc/G NFs were varied with respect to PMs as shown in **Figure 5(a)**. It was observed that (a) with an increase in spinning gap (cm), and high potential power supply (KV), the mean diameters (nm) of BF - NFs were reduced; and (b) with the increase in the rate of feed (ml h^{-1}), and the solution's resistance to the flow (cP), the mean diameters (nm) of the NFs were increased. The influence of ABC - Interaction between spinning gap (cm), rate of feed (ml h^{-1}) and high potential power supply (KV), AD - Interaction between spinning gap (cm) and solution's resistance to the flow (cP), D-Solution's resistance to the flow (cP), BC - Interaction between rate of feed (ml h^{-1}) and high potential power supply (KV), and AC - Interaction between spinning gap (cm) and high potential power supply (KV) were quite significant.

The contour plots (2D plots) of the mean diameters of NFs with respect to basic PMs were shown in **Figure 5(b)** and **(d)** [1]. **Figure 5(c)** and **(e)** [1] show the fitted model's predicted 3D response surface plots of the mean diameters (nm) of Cc/G NFs formed. The contributions of ABC-Interaction between spinning gap (cm), feed rate (mL/h), and power supply (KV), AD-Interaction between spinning gap (cm) and solution's resistance to the flow (cP), D-Solution's resistance to the flow (cP), BC-Interaction between feed rate (mL/h) and power supply (KV), and AC-Interaction between spinning gap (cm) and power supply (KV) had significant effects of 24 percent, 15.5 percent, 12 percent, and 11.5 percent, respectively, over the preparation of Cc/G NFs with minimum diameters. **Figure 5(f)** shows the optimized parameter settings. Shifting the red lines to find the optimum results of PMs within the range may be used to estimate the effects of important PMs on the mean diameter (nm) of Cc/G NFs. The composite desirability, D, in our case is 0.8129, which is similar to 1. The current response results are represented by the horizontal blue line (**Figure 5(f)**).

The mean diameter of UT - Cc/G NFs was predicted to be 189.6563 nm using a configured setting of 1.5 percent G and 1 percent Cc in 10 mL of 98 percent concentrated methanoic acid, with an electrospining unit with a power supply of 10 KV, a spinning gap from the emitter to collector drum of 15 cm, a feed rate of 0.1 mL/h, a solution's resistance to the flow of 65 cP, and a drum collector speed of 1000 rpm. The SEM image of Cc/G NFs with an mean diameter of 181 nm (181 ± 66 nm) synthesized under similar conditions using the same solution was shown in **Figure 4(b)**. As a result, the approximate diameter (nm) of Cc/G NFs in

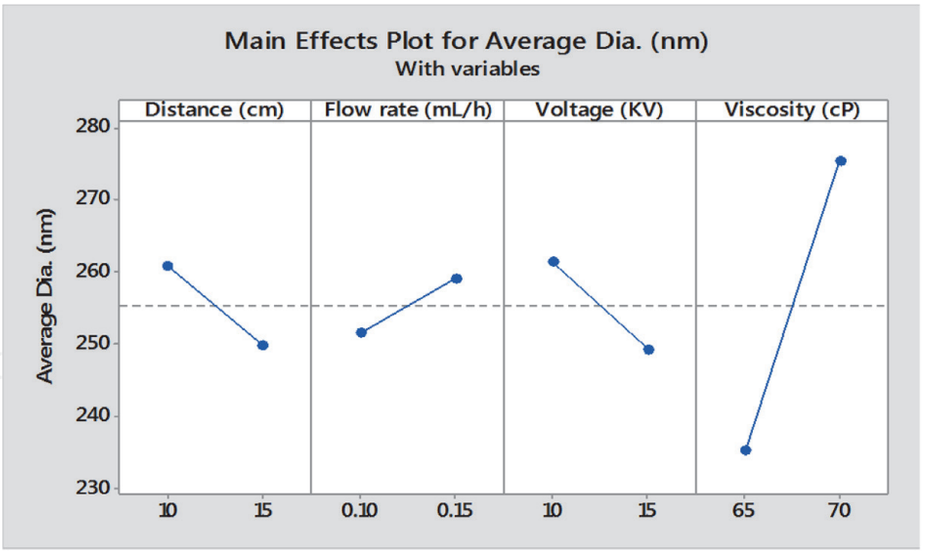

(a)

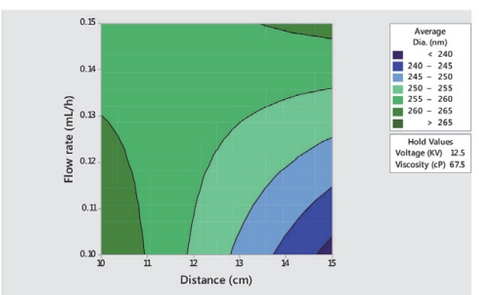

(b)

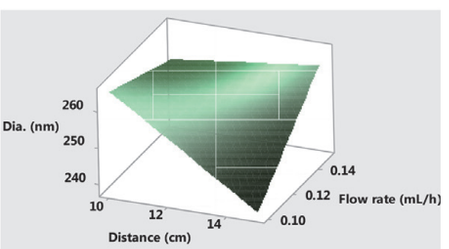

(c)

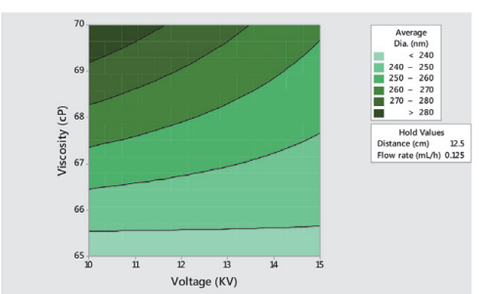

(d)

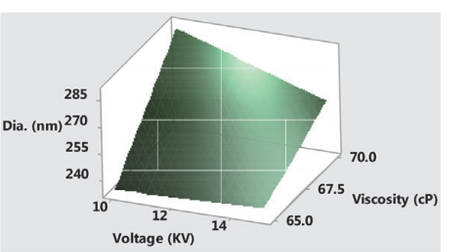

(e)

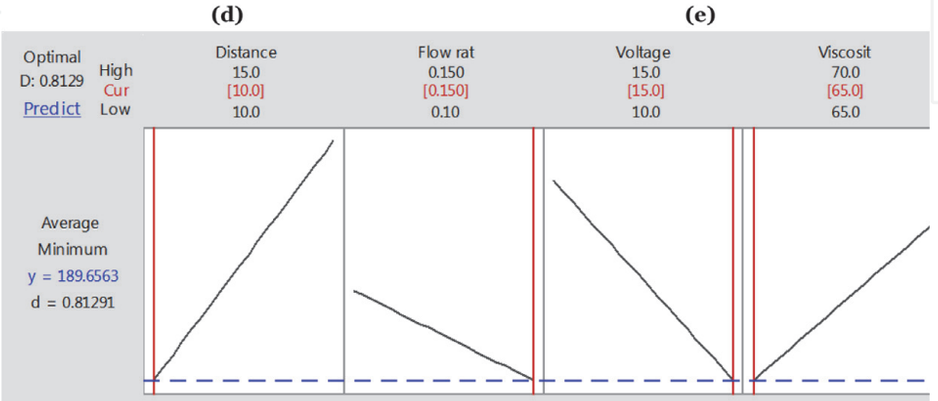

(f)

Figure 5.
Electrospining PMs optimization (reprinted with permission from ref. 1. Copyright 2020 IOP publishing). (a) Mean diameters of NFs versus PMs. (b), (d) two dimensional contour plots for mean diameter of NFs with respect to PMs. (c), (e) three dimensional plots for mean diameter of NFs with respect to PMs. (f) the study of optimized setting of PMs for synthesis of UT - NFs.

the optimization phase only differs by 8 percent from the prepared diameter, demonstrating the efficacy of the current study. Due to their high surface area to volume ratio in relation to length and diameter, we believe these LWs and UT - NFs with sufficient film porosity could be used in the healing process.

The optimum conditions for synthesizing the minimum mean diameter (181 ± 66 nm) of UT - Cc/G NFs were achieved (**Figure 4(b)**) in the study, which could be ideal for dressing diabetic chronic ulcers due to its specific properties such as LW, not harmful to living tissues, water absorbent, and fluid affinity.

Using the optimized environment of a polymeric solution, Sharjeel et al. [72] were effective in ESPNG, novel and hybrid polymeric nanofibrous mesh for dressing burn wounds after integrating gabapentin (a neuropathic pain killer) into polyethylene NFs and acetaminophen (a class of analgesics) into sodium alginate NFs (mixed in 80:20 blend proportion). In the healing process, the hybrid mechanism may be a safe option. Sharjeel et al. [73] synthesized ES - polyethylene oxide and chitosan NFs of 116 nm diameter (with a standard deviation of only 21 nm) using the response surface methodology with acetic acid and water (50:50, v/v) as the solvent (each dissolved separately in acetic acid and water solution in a 5 percent weight-to-volume ratio) (the ratio of polyethylene oxide and chitosan in the polymeric solution was 80:20).

4. Future researches

It is still a challenge to investigate the use of curcumin (Cc) loaded nanofibers (NFs) for efficient drug release during different stages of the healing process. Specific polymers for ES Cc NFs must be chosen based on the types of pharmaceutical to be released and the different stages of the healing process. That being said, the application of cytotoxic chemicals in drug delivery, especially during skin treatment, can negatively impact recent research findings. Current reviews of Cc in NFs have revealed a new area of research for the development of possible biomaterials for use in bone tissue science and medicine, diabetic chronic ulcer treatment, cancer treatment, and other applications [74–77].

5. Conclusion

Our analysis of Cc-based electrospun (ES) NFs underlines the importance, such as the relevance and need for BF - NFs and nanofibrous mats (NMs) in healing process, cancer care, tissue science and medicine, and other BAs, to inspire researchers interested in working in this cutting-edge area to solve various BAs with BF - NFs. To ease in the synthesis of UT - Cc/G NFs, the ESPNG mechanism (mathematical investigation of the process) was analyzed in detail in the first paper of the article.

The mechanism behind ESPNG was explored in this study as it was used to prepare curcumin/gelatin (Cc/G) NFs that could be used in the healing process. Gelatin (G) was chosen for the fiber system because it is not harmful to living tissues, as well as being water absorbent (fluid affinity), allowing for a moist healing process in the future. Since gelatin is commercially available at a low cost, it was an obvious option for the current study. The LW-UT and spongy NFs with mean diameter of 147 nm (147 ± 34 nm) were successfully synthesized using ESPNG at a higher power supply, such as 15 KV (at 10 cm distance, 0.15 mL/h feed rate, 65 cP solution's resistance to the flow, and drum collector speed of 1000 rpm)

with a solution containing 1.5 percent G and 1 percent Cc in 10 mL of 98 percent concentrated methanoic acid (**Figure 4(c)** and **Table 2**).

We came to the following conclusions after deciding the relative effects of the different ESPNG influences: (a) the effects of ABC-Spinning gap (cm), feed rate (mL/h), and higher potential power supply interaction (KV), AD-Interaction between spinning gap (cm) and solution's resistance to the flow (cP), D-Solution's resistance to the flow (cP), BC-Interaction between feed rate (mL/h) and high potential power supply (KV), and AC-Interaction between spinning gap (cm) and high potential power supply (KV) are 24 percent, 16 percent, 15.5 percent, 12 percent, and 11.5 percent, respectively, over the preparation of the Cc/G NFs' minimum diameters; (b) BCD-Feed rate (mL/h), high potential power supply (KV), and solution's resistance to the flow interaction (cP), ABCD-Spinning gap (cm), feed rate (mL/h), high potential power supply (KV), and solution's resistance to the flow interaction (cP), AB-Interaction between feed rate (mL/h) and spinning gap (cm), CD-High potential power supply (KV) and solution's resistance to the flow interaction (cP), C-High potential power supply (KV), A-Spinning gap (cm), and B-Feed rate (mL/h), BD-Interaction between feed rate (mL/h) and solution's resistance to the flow (cP) have a major influence on the preparation of Cc/G NFs with a minimum diameter; and (c) the diameter (nm) is affected by the ACD-Interaction between spinning gap (cm), high potential power supply (KV), and solution's resistance to the flow (cP) by just 0.05 percent, which is not important.

The 2^k factorial design of the experiment was used to investigate the effects of all four important PMs on the diameter of the NFs empirically. The MINITAB 17 programme was used to generate the results to investigate the difference in NFs' diameters as a function of input parameters. The differences in NFs diameters with respect to the critical PMs that were observed included (a) a higher spinning gap yielded lower diameters, (b) a higher potential power supply yielded lower diameters, (c) the diameter of the NFs increased with an increase in feed rate, and (d) the diameters of the NFs increased with an increase in solution's resistance to the flow.

Using the optimized setting of a solution containing 1.5 percent G and 1 percent Cc in 10 mL of 98 percent concentrated methanoic acid, and the electrospining machine with a high potential power supply of 15 KV, a spinning gap from the emitter to collector drum of 15 cm, a feed rate of 0.1 mL/h, solution's resistance to the flow of 65 cP, and a drum collector speed of 1000 rpm, the optimum condition for the production of UT - Cc/G NFs with an 189.6563 nm mean diameter was calculated. The approximate mean diameter (nm) of Cc/G NFs in the optimization phase differs by just 8 percent from the prepared mean diameter, i.e., 181 nm (181 ± 66 nm), demonstrating the efficacy of the current study.

Such UT - NFs with sufficient film porosity are not harmful to living tissues in nature, and it was suggested that they could be used in dressing problematic wounds, such as diabetic chronic ulcers, because they have unique properties, such as a high surface area to volume ratio and light weight, that allow for sustained Cc release during healing. The research paper that has been presented thus far is unique in that it covers (a) the entire ESPNG process (numerical investigations of the mechanism) to improve control over the preparation of UT - NFs, and (b) the applications of NMs (incorporating BF - NFs) that are currently in use. Eventually, the ESPNG PMs were optimized (to obtain UT - NFs) to prepare NMs for BAs such as the healing process (through sustained release of Cc during crucial hours of healing).

Author details

Nand Jee Kanu[1,2*], Eva Gupta[3,4], Venkateshwara Sutar[2], Gyanendra Kumar Singh[5] and Umesh Kumar Vates[3]

1 S. V. National Institute of Technology, Surat, India

2 JSPM NTC, Pune, India

3 Amity University, Noida, India

4 AGCE, Satara, India

5 Adama Science and Technology University, Adama, Ethiopia

*Address all correspondence to: nandssm@gmail.com

References

[1] Kanu NJ, Gupta E, Vates UK and Singh GK. Electrospinning process parameters optimization for biofunctional Curcumin/Gelatin nanofibers. Materials Research Express. 2020. (doi:10.1088/2053-1591/ab7f60)

[2] Khajavi R, Abbasipour M. Electrospinning as a versatile method for fabricating core–shell, hollow and porous nanofibers. Scientia Iranica F. 2012;19: 2029–2034.

[3] Skinner JL, Andriolo JM, Murphy JP and Ross BM. Electrospinning for nano- to mesoscale photonic structures. Nanophotonics. 2017; 6: 765–787.

[4] Huang ZX, Wu JW, Wong S-C, Qu JP and Srivatsan TS. The technique of electrospinning for manufacturing core–shell nanofibers. Materials and Manufacturing Processes. 2017. (https://doi.org/10.1080/10426914.2017.1303144)

[5] Ramakrishna S, Fujihara K, Teo WE, Yong T, ZuweiM and Ramakrishna R. Electrospun nanofibers: solving global issues. Materials Today. 2006;9:40–50.

[6] Pengcheng L, Yanbo L, Jinbo and Yao A. Review on the research status of massive production of nanofibers via electrospinning technology. Proceedings of the International Conference on Information Technology and Scientific Management. Scientific Research. 2010; 326–328.

[7] Reneker DH and Chun I. Nanometer diameter fibers of polymer, produced by electrospinning. Nanotechnology. 1996; 7:216–223.

[8] Jamil AM, Gary EW, DavidGS and Gary LB. Electrospinning of collagen nanofibers. Biomacromolecules. 2002;3: 232–238.

[9] Kriegel C, Arrechi A, Kit K, McClements DJ and JochenW. Fabrication, functionalization, and application of electrospun biopolymer nanofibers. Critical Reviews in Food Science and Nutrition. 2008; 48: 775–797.

[10] Shekh R, PrincetonCand Narayan B. Aloe vera for tissue engineering applications J. Funct. Biomater. 2017; 8. DOI:10.3390/jfb8010006.

[11] Merrell JG, McLaughlin SW, Tie L, LaurencinCT, Alex FC and Lakshmi SN. Curcumin loaded poly (ε-Caprolactone) nanofibers: Diabetic wound dressing with antioxidant and anti-inflammatory properties. Clin Exp Pharmacol Physiol. 2009; 36:1149–1156.

[12] Xinyi D, Juan L, Huaiyuan Z, Johannes W, Ursula H, Stefanie S, Carina P, Yi S, Machens HG and Arndt FS. Nano-formulated curcumin accelerates acute wound healing through Dkk-1-mediated fibroblast mobilization and MCP-1-mediated anti-inflammation. NPG Asia Materials. 2017; 9: e368.

[13] Narges F, Majid D, Jebraeel M and Azadeh S. Curcumin nanofibers for the purpose of wound healing. J. Cell. Physiol. 2018; 1–18.

[14] Mouthuy PA, Škoc MS, Gašparović AČ, Milković L, Carr AJ and Zarkovic N. Investigating the use of curcumin-loaded electrospun filaments for soft tissue repair applications. International Journal of Nanomedicine. 2017; 12:3977–3991.

[15] Chang SK, Doo HB, Kyung DG, Ki HL, In C.U. and Young HP. Characterization of gelatin nanofiber prepared from gelatin-formic acid solution. Polymer. 2005; 46: 5094–5102.

[16] Deng L, Kang X, Liu Y, Feng F and Hui Z. Characterization of gelatin/zein films fabricated by electrospinning versus solvent casting. Food Hydrocoll. 2018;74:324–332.

[17] Sadaf SG, Sima H and Hosein N. Fabrication and characterization of chitosan/gelatin/thermoplastic polyurethane blend nanofibers. Journal of Textiles and Fibrous Materials. 2018;1: 1–8.

[18] Ditpon K, Masaharu H, Mayuko O, Satoshi U, Masashi I, Tetsuya F and Hiroshi T. Preparation and characterization of electrospun gelatin nanofibers for use as nonaqueous electrolyte in electric double-layer capacitor. Journal of Nanotechnology. 2019. (https://doi.org/10.1155/2019/2501039)

[19] Lin L, Gu Y and Cui H. Novel electrospun gelatin-glycerin-ε-poly-lysine nanofibers for controlling *Listeria monocytogenes* on beef. Food Packaging and Shelf Life. 2018; 18: 21–30.

[20] Bazbouz MB, Liang H and Tronci G. A UV-cured nanofibrous membrane of vinylbenzylated gelatin-poly (ε-caprolactone) dimethacrylate co-network by scalable free surface electrospinning. Materials Science and Engineering C. 2018;91: 541–555.

[21] Yabing W, Haoxuan L, Yanhuizhi F, Peilin J, Jiansheng S and Chen H. Dual micelles-loaded gelatin nanofibers and their application in lipopolysaccharide-induced periodontal disease. International Journal of Nanomedicine. 2019; 14: 963–976.

[22] Jang HJ, Kim YM, Yoo BY and Seo YK. Wound-healing effects of human dermal components with gelatin dressing .J. Biomater. Appl. 2018; 32: 716–724.

[23] Aytac Z, Ipek S, Erol I, Durgun E and Tamer U. Fast-dissolving electrospun gelatin nanofibers encapsulating ciprofloxacin/ cyclodextrin inclusion complex. Colloids Surf. B Biointerfaces. 2019; 178:129–136.

[24] Piran M, Shiri M, Soufi ZM, Esmaeili E, Soufi ZM, Vazifeh SN, Mahboudi H, Daneshpazhouh H, Dehghani N and Hosseinzadeh S. Electrospun triple-layered PLLA/gelatin. PRGF/PLLA scaffold induces fibroblast migration. J. Cell. Biochem. 2019;1–13.

[25] Novickij V, Švedienė J, Paškevičius A, Markovskaja S, Girkontaitė I, Zinkevičienė A, Lastauskienė E and Novickij J. Pulsed electric field-assisted sensitization of multidrug-resistant *Candida albicans* to antifungal drugs. Future Microbiol.2018; 13: 535–546.

[26] Christina K, Alessandra A, Kevin K, McClements DJ and Weiss J. Fabrication, functionalization, and application of electrospun biopolymer nanofibers. Critical Reviews in Food Science and Nutrition. 2008; 48: 775–797.

[27] Liu X, Nielsen LH, Klodzinska SN, Nielsen HM, Qu H, Christensen LP, Rantanen J and Yang M.Ciprofloxacin-loaded sodium alginate/poly (Lactic-Co-Glycolic Acid) electrospun fibrous mats for wound healing. Eur. J. Pharm. Biopharm. 2018; 123: 42–49.

[28] Chouhan D, Janani G, Chakraborty B, Nandi S K and Mandal BB. Functionalized PVA-silk blended nanofibrous mats promote diabetic wound healing via regulation of extracellular matrix and tissue remodeling. J. Tissue Eng. Regen. Med. 2018;12: e1559–e1570.

[29] Gizaw M, Thompson J, Faglie A and Lee SY. Electrospun fibers as a dressing material for drug and biological agent delivery in wound healing applications. Bioengineering. 2018;5:1–33.

[30] Tonda-Turo C, Ruini F, Ceresa C, Gentile P, Varela P, Ferreira AM, Fracchia L and Ciardelli G. Nanostructured scaffold with biomimetic and antibacterial properties for wound healing produced by 'green electrospinning approach Colloids Surf. B. 2018;1: 1–34.

[31] Mindru TB, Mindru IB, Malutana T and Turab V. Electrospinning of high concentration gelatin solutions. Journal of Optoelectronics and advanced Materials. 2007; 9: 3633–3638.

[32] Maleknia L and Majdi ZR. Electrospinning of gelatin nanofiber for biomedical application. Oriental Journal of Chemistry. 2014; 30: 2043–2048.

[33] Chen HC, Jao WC and Yang MC. Characterization of gelatin nanofibers electrospun using ethanol/formic acid/ water as a solvent. Polymer Advanced Technologies. 2008;20:98–103.

[34] Vitalij N, Eglė L, Gediminas S, Irutė G, Auksė Z, Jurgita Š, Algimantas P, Svetlana M and Jurij N. Low concentrations of acetic and formic acids enhance the inactivation of *Staphylococcus aureus* and *Pseudomonas aeruginosa* with pulsed electric fields. BMC Microbiology. 2019;19. (https:// doi.org/10.1186/s12866-019-1447-1.)

[35] Constantin T, Konstantinos D, Zacharias DS, Sophia H, Han Z, Liu ZL, Wyche JH and Pantazis P. Metabolism and anticancer activity of the curcumin analogue, dimethoxycurcumin. Clin Cancer Res. 2007;13:1269–1277.

[36] Ramírezagudelo R, Scheuermann K, Galagarcía A, Monteiro A, Pinzón-García AD, Cortés ME and Sinisterra RD. Hybrid nanofibers based on poly-caprolactone/gelatin/ hydroxyapatite nanoparticles-loaded doxycycline: effective anti-tumoral and antibacterial activity. Materials Science and Engineering C. 2018;83: 25–34.

[37] Wong K, Ngai S, Lee L, Goh B, Chan KG and Chuah LH. Curcumin nanoformulations for colorectal cancer: a review Front.Pharmacol. 2018;10: 152.

[38] Chen Y, Du Q, Guo Q, Huang J, Liu L, Shen X and Peng J. A W/O emulsion mediated film dispersion method for curcumin encapsulated pH-sensitive liposomes in the colon tumor treatment. Drug Dev. Ind. Pharm. 2018; 1–10.

[39] Ferri C, West K, Otero K and Kim YH. Effectiveness of curcumin for treating cancer during chemotherapy. Altern Complement Ther. 2018; 24: 13–18.

[40] Javadi S, Rostamizadeh K, Hejazi J, Parsa M and Fathi M. Curcumin mediated down-regulation of alphaV beta3 integrin and upregulation of pyruvate dehydrogenase kinase 4 (PDK4) in Erlotinib resistant SW480 colon cancer cells. Phytother Res. 2018; 32: 355–364.

[41] Marjaneh RM, Rahmani F, Hassanian SM, Rezaei N, Hashemzehi M, Bahrami A, Ariakia F, Fiuji H, Sahebkar A, Avan A, Khazaei M. Phytosomal curcumin inhibits tumor growth in colitis-associated colorectal cancer. J Cell Physiol. 2018; 233: 6785–6798.

[42] Sesarman A, Tefas L, Sylvester B, Licarete E, Rauca V, Luput L, Patras L, Banciu M and Porfire A. Anti-angiogenic and antiinflammatory effects of long-circulating liposomes co-encapsulating curcumin and doxorubicin on C26 murine colon cancer cells. Pharmacol Rep. 2018; 70: 331–339.

[43] Enas A, Clive JR, Rozita R, Kah HY and Eng KS. Pharmacokinetic and anti-colon cancer properties of curcumin-containing chitosan-pectinate composite nanoparticles. Journal of Biomaterials Science Polymer Edition. 2018. (https:// doi.org/10.1080/09205063.2018.1541500)

[44] Yasmine A, Kaoru O, Ahmed A, Hirokazu S, Kawai T, Lim CT, Kumar V, Okaya S, Kato K, Hiyama E, Yanagida T, Masujima T, Shimizu Y, Honda K. Live single cell mass spectrometry reveals cancer-specific metabolic profiles of

circulating tumor cells. Cancer Sci. 2019;110: 697–706.

[45] Rafael CC, Laura C, Gloria P, Amelia D, Juan ML-R, Consolación M and Jose P. Electrospun nanofibers: recent applications in drug delivery and cancer therapy. Nanomaterials. 2019; 9: 656. (https://dx.doi.org/10.3390%2Fnano9040656)

[46] Feifei W, Zhaoyang S, Jing Y and Lan X. Preparation, characterization and properties of porous PLA/PEG/ Curcumin composite nanofibers for antibacterial application Nanomaterials. 2019;9: 508. (https://dx.doi.org/10.3390%2Fnano9040508)

[47] Wang J and Windbergs M. Influence of polymer composition and drug loading procedure on dual drug release from Plga:Peg electrospun fibers. Eur. J. Pharm. Sci. 2018; 124: 71–79.

[48] Negut I, Grumezescu V and Grumezescu AM. Treatment strategies for infected wounds Molecules. 2018; 2329: 1–23.

[49] Hoang MS, Doan NH and Huynh DP. Fabrication of curcumin loaded nano polycaprolactone/chitosan nonwoven fabric via electrospinning technique. Journal of Science and Technology. 2017; 55: 99–108.

[50] Abdollahi E, Momtazi AA, Johnston TP and Sahebkar A. Therapeutic effects of curcumin in inflammatory and immune mediated diseases: a nature-made jack-of-all-trades? Journal of Cellular Physiology. 2018; 233: 830–848.

[51] Dai J, Gu L, Su Y, Wang Q, Zhao Y, Chen X, Deng H, Li W, Wang G and Li K. Inhibition of curcumin on influenza A virus infection and influenzal pneumonia via oxidative stress, TLR2/4, p38/JNKMAPK and NF-κB pathways. International Immunopharmacology. 2018; 54: 177–187.

[52] Panahi Y, Khalili N, Sahebi E, Namazi S, Simental-Mendía LE, Majeed M and Sahebkar A. Effects of curcuminoids plus piperine on glycemic, hepatic and inflammatory biomarkers in patients with type 2 diabetes mellitus: A randomized double-blind placebo controlled trial. Drug Research. 2018;68: 403–409.

[53] Zhao Y, Liu JG, ChenWM and Yu AX. Efficacy of thermosensitive chitosan/β-glycerophosphate hydrogel loaded with βcyclodextrin-curcumin for the treatment of cutaneous wound infection in rats Experimental and Therapeutic Medicine. 2018;15: 1304–1313.

[54] Mamidi N, Romo IL, Gutiérrez HML, Barrera EVand Alex EZ. Development of forcespun fiber-aligned scaffolds from gelatin–zein composites for potential use in tissue engineering and drug release. MRS Communications. 2018; 1–8.

[55] Mamidi N, Romo IL, Barrera EV and Alex EZ. High throughput fabrication of curcumin embedded gelatin-polylactic acid forcespun fiber-aligned scaffolds for the controlled release of curcumin. MRS Communications. 2018; 1–9.

[56] Ravikumar R, Ganesh M, Senthil V, Ramesh YV, Jakki SL and Eun YC. Tetrahydro curcumin loaded PCL-PEG electrospun transdermal nanofiber patch: Preparation, characterization, and in vitro diffusion evaluations. J. Drug Del. Sci. Tech. 2018; 44: 342–348.

[57] Weilan Y, Dingsheng W, Dake C, Juntao Z, Gan H, Jiang F, Liu X, Lao B, Yu W, Guan Y and Zhong G. Simultaneous determination of curcumin, tetrahydrocurcumin, quercetin, and paeoniflorin by UHPLC-MS/MS in rat plasma and its application to a pharmacokinetic study. Journal of Pharmaceutical and Biomedical Analysis. 2019; 172:58–66.

[58] Wang Y and Xu L. Preparation and characterization of porous core-shell

fibers for slow release of tea polyphenols. Polymers. 2018; 10: 144.

[59] Lu H, Qiu Y, Wang Q, Li G and Qufu W. Nanocomposites prepared by electrohydrodynamics and their drug release properties. Materials Science and Engineering C. 2018;91: 26–35.

[60] Zhang L, Wang Z, Xiao Y, Liu P, Shige W, Yili Z, Mingwu S and Xiangyang S. Electrospun PEGylated PLGA nanofibers for drug encapsulation and release. Mater. Sci. Eng.C. 2018;91: 255–262.

[61] Mostafalu P, Tamayol A, Rahimi R, Ochoa M, Akbar K, Gita K, Iman KY, Sara B, Mehmet RD, Babak Z, Sameer RS, Ali K. Smart Bandage for Monitoring and Treatment of Chronic Wounds. Small. 2018; 14: 1703509.

[62] Haley RM and Von RHA. Localized and targeted delivery of Nsaids for treatment of inflammation: a review. Exp. Biol. Med. 2018.

[63] Cheng H, Yang X, Che X, Yang M and Guangxi Z. Biomedical application and controlled drug release of electrospun fibrous materials. Materials Science and Engineering C. 2018;90: 750–763.

[64] Hao S, Zhang Y, Meng J, Liu J, Wen T, GuNand XuH. Integration of a superparamagnetic scaffold and magnetic field to enhance the wound-healing phenotype of fibroblasts. ACS Appl. Mater. Interfaces. 2018; 10 22913–22923.

[65] Abudula T, Gzara L, Simonetti G, Alshahrie A, Salah N, Morganti P, Chianese A, Fallahi A, Tamayol A, Bencherif SA, Memic A. The Effect of Poly (Glycerol Sebacate) Incorporation within Hybrid Chitin–Lignin Sol–Gel Nanofibrous Scaffolds. Materials. 2018; 11: 451.

[66] Novickij V, Zinkevičienė A, Perminaitė E, Čėsna R, Eglė L, Algimantas P, Jurgita Š, Svetlana M, Jurij N and Irutė G. Noninvasive nanosecond electroporation for biocontrol of surface infections: an in vivo study. Sci. Rep. 2018;8: 14516.

[67] Mi Y, Xu J, Tang X, Bian C, Hongliang L, Qiyu Y and Junying T. Scaling relationship of in vivo muscle contraction strength of rabbits exposed to high-frequency nanosecond pulse bursts Technol. Cancer Res. Treat. 2018; 17.

[68] Yeo YL and Friend RJ. Electrospinning carbon nanotube polymer composite nanofibers. J. Exp. Nanosci. 2006; 1 : 177–209.

[69] Rafiei S, Maghsoodlou S, Saberi M, Lotfi S, Motaghttalab V, Noroozi B and Haghi AK. New Horizons in modeling and simulation of electrospun nanofibers: a detailed review. Cellulose Chem. Technol. 2014; 48: 401–424.

[70] Mir RM, Mehdi R and Farhad S. Investigation of effect of electrospinning parameters on morphology of polyacrylonitrile/ polymethyl methacrylate nanofibers: a box-behnken based study Journal of Macromolecular Science, Part B: Physics. 2015. (https://doi.org/10.1080/ 00222348.2015.1042628)

[71] Vince B and Xuejun W. Effect of electrospinning parameters on the nanofiber diameter and length. Materials Science and Engineering C. 2009;29: 663–668.

[72] Montgomeryv DC. Design and Analysis of Experiments. (New York: Wiley) Student Edition. 2013. 8th Edition.

[73] Ross PJ. Taguchi techniques for quality engineering. (New York: McGraw Hill Book Company). 1989.

[74] Sharjeel A, Tanveer H, Ahsan N, Abdul Z and Nabyl K. A novel double-

layered polymeric nanofiber-based dressing with controlled drug delivery for pain management in burn wounds Polym. Bull. 2019. (https://doi.org/10.1007/s00289-019-02727-w)

[75] Sharjeel A, Tanveer H, Ahsan N, Abdul Z, Seeram R, Misbah H and Nabyl K. Enhanced antibacterial activity of PEO-chitosan nanofibers with potential application in burn infection management. Int. J. Biol. Macromol. 2019; 135: 1222–1236.

[76] Gang G, ShaoZhi F, LiangXue Z, Hang L, Min F, Feng L, ZhiYong Q and YuQuan W. Preparation of curcumin loaded poly(ε- caprolactone)-poly (ethylene glycol)-poly(ε-caprolactone) nanofibers and their in vitro antitumor activity against Glioma 9L cells. Nanoscale. 2011; 3: 3825.

[77] Sharjeel A, Tanveer H, Zulfiqar A R and Ahsan N. Current applications of electrospun polymeric nanofibers in cancer therapy Materials Science and Engineering C. 2019; 97: 966–977.